Nature. Author manuscript; available in PMC 2014 December 12.

Published in final edited form as:
Nature. 2014 June 12; 510(7504): 235–240. doi:10.1038/nature13420.

Targeted Genome Editing in Human Repopulating Hematopoietic Stem Cells

Pietro Genovese[1], **Giulia Schiroli**[#1,2], **Giulia Escobar**[#1,2], **Tiziano Di Tomaso**[1], **Claudia Firrito**[1], **Andrea Calabria**[1], **Davide Moi**[1,*], **Roberta Mazzieri**[1,*], **Chiara Bonini**[3], **Michael C. Holmes**[4], **Philip D. Gregory**[4], **Mirjam van der Burg**[5], **Bernhard Gentner**[1,2], **Eugenio Montini**[1], **Angelo Lombardo**[1,2,¶], and **Luigi Naldini**[1,2,¶]

[1]TIGET, San Raffaele Telethon Institute for Gene Therapy, San Raffaele Scientific Institute, Milan, Italy [2]Vita Salute San Raffaele University, Milan, Italy [3]Experimental Hematology Unit, San Raffaele Scientific Institute, Milan, Italy [4]Sangamo BioSciences Inc., Richmond, CA, United States. [5]Dept. of Immunology Erasmus MC, University Medical Center, Rotterdam, The Netherlands

[#] These authors contributed equally to this work.

Abstract

Targeted genome editing by artificial nucleases has brought the goal of site-specific transgene integration and gene correction within the reach of gene therapy. However, its application to long-term repopulating Hematopoietic Stem Cells (HSCs) has remained elusive. Here we show that poor permissiveness to gene transfer and limited proficiency of the homology directed DNA repair pathway constrain gene targeting in human HSCs. By tailoring delivery platforms and culture conditions we overcame these barriers and provide stringent evidence of targeted integration in human HSCs by long-term multilineage repopulation of transplanted mice. We demonstrate the therapeutic potential of our strategy by targeting a corrective cDNA into the IL2RG gene of HSCs from healthy donors and a subject with X-linked Severe Combined Immunodeficiency (SCID-X1). Gene edited HSCs sustained normal hematopoiesis and gave rise to functional lymphoid cells that possess a selective growth advantage over those carrying disruptive IL2RG mutations. These results open new avenues for treating SCID-X1 and other diseases.

Correspondence to: naldini.luigi@hsr.it.
[¶]These Authors share senior authorship.

Author Contributions: PG designed experiments, performed research, interpreted data and wrote the manuscript. GS and GE performed research and interpreted data. TDT performed mRNA production. CF characterized the corrective cDNA. AC and EM performed bioinformatics analysis of ZFN specificity. RM and DM developed the NSG human tumor rejection model. CB contributed to the T cell studies. MvdB provided SCID-X1 patient cells. MCH and PDG provided ZFNs, interpreted data and edited the manuscript. BG set up culture conditions for HSC maintenance. AL and LN designed and supervised research, interpreted data and wrote the manuscript. LN coordinated the study.

[*]Present address: The University of Queensland Diamantina Institute, Translational Research Institute, Brisbane, Queensland 4102, Australia

MCH and PDG are employees of Sangamo BioSciences Inc. PG, AL, LN, MCH and PDG filed a patent application on the protocol for targeted integration in human HSPC.

Europe PMC Funders Author Manuscripts

Hematopoietic Stem Cells (HSC)-based gene therapy has provided therapeutic benefit in primary immunodeficiencies[1,2], thalassemia[3] and leukodystrophies[4,5]. Whereas more advanced vectors, such as lentiviral vectors (LV)[6] have shown improved safety and efficacy, the risk of insertional mutagenesis[7,8] and unregulated transgene expression[9,10] remains a concern when using semi randomly integrating vectors. These adverse effects may trigger oncogenesis, toxicity or elimination of the gene-modified cells.

Artificial endonucleases, such as Zinc Finger Nucleases (ZFNs)[11], Transcription Activator-Like Effector Nucleases (TALENs)[12], and RNA-guided nucleases (CRISPR/Cas)[13] brought the possibility of gene targeting within the reach of gene therapy[14,15]. These nucleases are used to efficiently and specifically target a DNA Double Strand Break (DSB) to a preselected genomic site[13,16,17]. According to the repair process that seals the break[18], the outcome can be disruption, reconstitution or editing of the original sequence. If the DSB is sealed by the error-prone Non-Homologous End-Joining (NHEJ) pathway, insertions and deletions (indels) are common[19-21]. If the DSB is sealed by the high-fidelity Homology Directed Repair (HDR) pathway, which acts preferentially during the S/G2 phase, the targeted sequence can be edited by providing an exogenous DNA template flanked by homologous sequences to the nuclease target site. Targeted editing allows integrating an expression cassette into a safe genomic harbor[22,23], or correcting disease-causing mutations by inserting a functional copy of the affected gene downstream its own promoter[14,24]. Gene correction, as opposed to gene replacement, may not only restore the function but also the physiological expression of the gene, a long-sought goal of gene therapy.

Whereas gene disruption by ZFNs has been shown in human hematopoietic stem/progenitor cells (HSPC) assayed by repopulation of SCID mice[20], targeted gene editing in these cells has not been reported. Here, we identify and overcome major constraints limiting gene targeting in HSPCs and provide proof-of-efficacy for this approach by functional reconstitution of the *IL2RG* gene, whose mutations are responsible for X-linked Severe Combined Immunodeficiency (SCID-X1).

Site-specific integration in human HSPC

We developed a protocol for delivery of ZFNs and donor DNA template into human cord blood (CB) CD34+ cells by mRNA electroporation and Integrase-Defective LV (IDLV), and targeted integration of a GFP cassette into the *AAVS1* "safe harbor"[22] or a mutational hotspot of *IL2RG*[14,15] (Fig. 1a,b and Extended Data Fig. 1). This protocol yielded on average 5% GFP+ cells in liquid culture and colony-forming cells (CFC) assays and high percentages of indels in the respective ZFNs target sites, although after a transient cell loss (Fig. 1c and Extended Data Fig. 2a-e). PCR analysis and Southern blot showed integration of the GFP cassette at the intended targets in >90% of the GFP+ colonies (n=89) and in induced Pluripotent Stem cells obtained by reprogramming the GFP+ sorted cells (Fig. 1d,e and Extended Data Fig. 2f,g). We then transplanted the CD34+ cells treated for *AAVS1* or *IL2RG* gene targeting into NSG mice and found human cells engraftment in all mice (Fig. 2a). In the first 8 weeks post-transplant, 95% of the mice had circulating GFP+ cells (mean 6.2±1.3%; Fig. 2b), while only 42% of the mice maintained long-term GFP marking. End-point analyses performed on the peripheral blood (PB), spleen and bone marrow (BM)

showed that GFP+ cells were present within all human hematopoietic lineages, including lymphoid and myeloid cells, and erythroid precursors (mean 2±0.8%; Fig. 2c). Similar frequencies of GFP+ cells were found among primitive and committed progenitors in the BM (mean 2.2±0.9%; Fig. 2d). PCR analyses confirmed targeted integration in human lymphoid, myeloid and CD34+ cells from the spleen and BM of representative mice (Fig. 2e). CFC assays on CD34+ cells from BM showed GFP+ myeloid and erythroid colonies (Fig. 2f) with targeted integration (Fig. 2e). Analysis of BM cells showed the occurrence of NHEJ-mediated indels in the ZFN target site in the majority of mice (64%; Fig. 2g) at higher levels than observed for GFP marking, indicating that DNA DSB induction and repair by either HDR or NHEJ is compatible with hematopoietic repopulation. Overall, these data show that our gene targeting protocol achieves site-specific integration in human multipotent long-term NSG repopulating cells (SRC), surrogate readouts of HSC.

Low targeting efficiency in HSPC

The *in vivo* studies revealed that only ~40% of mice had on average 2% human GFP+ cells long-term. These figures appear lower than expected from transplanting CD34+ cells with ~5% targeting efficiency *in vitro* (Suppl. Information) and suggest that either SRCs are targeted less efficiently than the bulk CD34+ cells, or the gene targeted SRCs have a competitive disadvantage *in vivo*. We thus compared the percentages of GFP+ cells among different subpopulations of cultured CD34+ cells, prospectively identified by surface markers[25] as primitive (CD34+133+90+), early (CD34+133+90−) and committed (CD34+133−) progenitors and the differentiated cells (CD34−, Fig. 3a left panel). We found a decreasing frequency of GFP+ cells when moving from the differentiated cells up the progenitor hierarchy. In primitive cells the percentage of GFP+ cells was 20-fold lower than that measured in differentiated cells. We thus investigated the potential rate-limiting steps for gene targeting in primitive cells (Extended Data Fig. 3a-d). Transgene expression upon mRNA electroporation was similar among the subpopulations or slightly lower for the primitive cells. The level of NHEJ induced at the ZFN target site was higher in the primitive cells and progressively lower in committed and differentiated cells. This difference, however, diminished with time in culture, potentially due to the loss of some treated primitive cells. Indeed, induction of apoptosis was higher in this subset. Taken together these data suggest that the primitive cells are more sensitive to our treatment and less permissive to HDR and/or donor template delivery.

Tailored conditions improved HSC gene targeting

Because cell cycle progression is a requirement of HDR and activation of the primitive progenitors may require longer stimulation, we postponed the gene targeting procedure to the 3rd day of culture (Fig. 3b). At this time, the cells are also likely to become more permissive to LV transduction. Because increasing time in culture promote differentiation, we added the Aryl Hydrocarbon Receptor Antagonist (StemRegenin 1, SR1)[26] and/or 16,16 dimethylprostaglandin E2 (dmPGE2)[27,28] to the culture to better preserve stem and early progenitor cells (Fig. 3c). The delayed protocol increased significantly (≥2-fold) the percentage of GFP+ cells in primitive cells (Figure 3a, right panels). SR1 slightly reduced the percentage of GFP+ cells observed within each subpopulation but increased the yield of

GFP+ CFC and early progenitors, consistently with the increased proportion of immature cells in SR1-treated cultures (Fig. 3d,e and Extended Data Fig. 3e). The addition of dmPGE2 increased the percentage of GFP+ cells in all subpopulations when used alone and showed additive effects with SR1. Importantly, both the delayed treatment and the addition of SR1 and dmPGE2 increased the fraction of mice long-term engrafted with GFP+ cells, which reached 100% when used in combination (Fig. 3f). Human cell engraftment significantly increased after SR1 addition to the culture (Fig. 3g) and was stable long-term (Extended Data Fig. 4a,b). Consistently with the increased GFP marking observed *in vitro* in the primitive cells, the mean percentage of GFP+ cells long-term engrafted *in vivo* increased with all types of delayed treatments (Fig. 3h). GFP+ cells contributed to multiple lineages and to the progenitor compartment in most mice (Extended Data Fig. 4c,d). Molecular analyses on BM cells showed evidence of targeted integration (Extended Data Fig. 4e). Serial transplant of purified CD34+ cells from the BM of primary mice showed engraftment and differentiation of targeted GFP+ cells in secondary recipients (Extended Data Fig. 4f,g). Overall, these data indicate that by tailoring experimental conditions we could improve the yield and frequency of targeted long-term SRC.

Targeted gene editing of *IL2RG* in HSPC

In the experiments described in Fig. 3g,h, the gene targeting construct was designed to insert a cDNA comprising exon 5 to 8 of *IL2RG* together with the GFP cassette into the *IL2RG* gene and used on CD34+ cells from healthy male donors (Fig.4a). In this way, the cDNA is transcribed from the endogenous *IL2RG* promoter and spliced to its upstream exons, thus providing a platform for correcting all SCID-X1 causing mutations downstream of exon 4. In order to assess functional reconstitution of the targeted gene, we challenged the repopulated mice with a human tumor cell line (MDA-MB 231) engineered to express human IL-7, IL-15 and GM-CSF (Fig. 4b). We previously reported that this challenge leads to improved reconstitution of functional human T and NK cells that eventually reject the tumor graft[29]. T and NK cells are strictly dependent on IL2RG expression for survival and activity and are absent in SCID-X1. Upon tumor challenge, we observed a massive (mean 130±40-fold) expansion of the human T and NK lineages in the repopulated mice (Extended Data Fig. 5). GFP+ T and NK cells expressed IL2RG on the cell surface (Fig. 4c) and expanded similarly to their GFP negative counterparts in all mice (Fig. 4d). All repopulated mice effectively rejected the allogeneic tumor, at variance with non-transplanted mice, underscoring the development of a functional human immune system (Fig. 4e). Whereas myeloid cells sorted from the mice showed high levels of NHEJ at the targeted *IL2RG* site, comparable to those observed in the CD34+ cells pre-transplant, B cells showed very little, and T and NK cells virtually none (Fig. 4f). These findings reflect the dramatic counter selection of lymphoid cells carrying a disrupted *IL2RG*, as it naturally occurs with inherited SCID-X1 alleles, and confirm the functionality of the reconstituted gene in the expanded GFP+ cells. We then assessed the T-cell receptor repertoire of lymphocytes from the engrafted mice and found substantial diversity with almost overlapping polyclonal pattern between the GFP+ and GFP-sorted cell subsets (Fig. 4g and Extended Data Fig. 6). The GFP + and GFP− T cells expanded *ex vivo* after polyclonal stimulation with the same kinetics in the presence of γ-chain dependent cytokines (IL-7 and IL-15), and proliferated to a similar

Europe PMC Funders Author Manuscripts

extent in response to the allogeneic MDA-MB 231 cells (Fig. 4h,i and Extended Data Fig. 7a). GFP+ and GFP− T cells were similarly comprised of CD8 and CD4 cell subsets, with a majority of cells showing effector phenotypes (Extended Data Fig. 7b,c). Consistently, both GFP+ and GFP− cells robustly produced γIFN and IL-2 after PMA-ionomycin stimulation or when co-cultured with the allogeneic tumor at different effector/target ratios (Extended Data. Fig. 7d,e). Molecular analyses proved that nearly all GFP+ cells contained targeted integration into *IL2RG* (Fig. 4j). We then measured the phosphorylation of two downstream effectors in the signaling cascade of γ-chain coupled receptors (Fig. 4k and Extended Data Fig. 8). The targeted T cells displayed similar kinetics and extent of phosphorylation of STAT5 and AKT as their GFP-counterparts after stimulation with increasing IL-15 and IL-2 doses. Overall, these data prove functional reconstitution of the edited *IL2RG* gene, which supported lymphopoiesis and mature T-cell function indistinguishably from the wild-type allele.

Specificity of *IL2RG* ZFNs on the HSC genome

We previously performed a genome-wide screening in K562 cells to identify potential off target sites of the *IL2RG* ZFNs used in this study[16] and found a low rate of indels in few genomic loci bearing homology to the intended target site. We then determined whether these sites were also affected in the HSPC treated here with ZFNs containing the same *IL2RG* DNA binding domains but coupled to improved obligate heterodimeric FokI domains. We deep sequenced the genomic regions encompassing the identified potential target sites on treated CD34+ cells cultured in vitro and on human cells from the BM of long-term engrafted NSG mice (Table 1 and Extended Data Fig. 9). The intended *IL2RG* target site showed 45 to 61% indels rate in the *in vitro* cultured cells and 20 to 43% in the *in vivo* engrafted cells. However, we detected indels only in 2 in vitro samples (at 0.17 to 0.7%) for the top 2 previously identified off target sites, while from the *in vivo* samples we found just one site with evidence of NHEJ (at 0.02%). Deep sequencing of all other putative off-target sites gave results not statistically different from the background error rate, which limits detection at 0.01% in our analysis (see Suppl. Information). The elimination of detectable off-target activity at some previously identified sites is consistent with the adoption of obligate heterodimeric FokI variants in this study, which would detarget activity from sites requiring ZFN homodimers. This analysis demonstrates a high specificity for the ZFNs used, evidenced by the 100 fold ratio between activities at the intended target site vs. the top identified off target site. It is possible, however, that additional off-target sites exist, which have not been identified by our previous screening.

IL2RG gene correction in SCID-X1 HSPC

We applied the optimized protocols developed for CB to CD34+ cells from adult BM and obtained an overall gene targeting efficiency of 6±0.5% (n=4 donors) and a high rate of indels induced at either the *AAVS1* or *IL2RG* ZFNs target sites (Fig. 5a). Targeting was less efficient in the more primitive populations although reaching similar values as those observed for CB cells. Xenotransplantation proved the long-term multilineage repopulation capacity of the targeted cells, with all transplanted NSG mice bearing GFP+ cells at frequencies comparable to those observed with CB cells (Fig. 5b). Based on these results,

we then tested our gene correction strategy on BM CD34+ cells from a symptomatic four-month old SCIDX1 patient bearing a missense mutation in *IL2RG* Exon 7 (c.865C>T; R289X). As expected for this mutation, blood sampling or BM harvest from the patient did not show any T or NK cells (Extended Data Fig. 10a,b). From 3 to 11% of the treated cell progeny became GFP+, depending on primitive vs. committed progenitor status (Fig. 5c). CFC assays yielded 3 GFP+ colonies out of ~100 scored (Extended Data Fig. 10c). Flow cytometry showed normal expression of the γ-chain protein in the myeloid progeny of the GFP+ CFCs (Fig. 5d). PCR analyses of these colonies proved targeted integration into *IL2RG* leading to expression of the expected fusion transcript between the corrective cDNA and the upstream endogenous exons (Fig. 5e,f and Suppl. Information). Overall, this data shows reconstitution of a functional *IL2RG* gene upon targeted editing of a SCID-X1 allele in HSPC.

Discussion

Here we developed a strategy for targeted genome editing in human long-term repopulating HSCs and exploited it to insert transgenes into a genomic safe harbor or downstream of the promoter of an endogenous gene to reconstitute its functional expression. By the latter approach, we demonstrate correction of the defective *IL2RG* gene in HSPC from a subject with SCID-X1. As we obtained consistent results when targeting two different loci, we expect that our genome editing strategy can be used to target a variety of genomic sites. As the procedure employs a combination of IDLV infection and mRNA electroporation to deliver donor template and ZFNs, it has the potential to be applicable to a range of other genome editing tools.

We found that primitive cells are more sensitive than committed progenitors to the cytotoxicity of the gene targeting procedure and less proficient at performing HDR, likely because of their quiescence or slow cycling. These findings are consistent with reports showing delayed DNA repair and enhanced apoptosis after γ-radiation in human HSC as compared to progenitors[30] and preferential repair of DNA DSBs by NHEJ in quiescent murine HSC[31]. By delaying the time of treatment and exploiting compounds reported to support *ex vivo* maintenance and expansion of HSCs[26-28], we were able to partially relieve the block to HDR. This effect is likely due to an increased transit through the S/G2 phases of the cell cycle, when HDR can occur, and, possibly, up-regulation of its endogenous machinery. Other beneficial effects might be increased permissiveness to gene delivery, more efficient mRNA translation and reduced growth arrest and apoptosis in response to the gene targeting procedure. As improved procedures for *ex vivo* HSC expansion become available, they might increase the yield of gene targeted cells and allow their selection before *in vivo* administration. This would enable wide application of safe harbor sites, such as *AAVS1*, for robust expression of therapeutic transgenes[22,23].

When applied to the functional correction of *IL2RG* in HSCs, we show that our strategy is compatible with normal development of the lymphoid lineages. *IL2RG* edited lymphoid cells repopulated the mice and responded to γ-chain-dependent cytokines indistinguishably from their unedited counterparts. On the contrary, lymphoid cells carrying NHEJ-mediated *IL2RG* inactivation were counter-selected in the mice, phenocopying the SCID-X1 disease[1].

This disease may be suitable for the clinical translation of targeted gene correction since prior clinical studies have demonstrated the potential efficacy but also the risks of HSC gene therapy using early generation vectors[7,8]. Whereas our strategy should abrogate the risk of insertional mutagenesis and the concern for unregulated transgene expression, it remains to be established whether a potentially limiting amount of targeted HSPCs would enable effective and safe correction of SCID-X1 in humans (even though both HSC and progenitors, which are more efficiently targeted, would help repopulating the absent lymphoid lineages). Another concern is with the potential ZFNs off target activity, although our analysis showed a high specificity for the *IL2RG* ZFNs used in this study. Overall, we envisage a fairly straightforward path to clinical translation of our strategy, considering that GMP manufacturing of LV and mRNA electroporation are already established. Moreover, infusion of autologous gene targeted cells could be performed without pharmacological conditioning, taking advantage of the selective advantage of the corrected cells.

Methods

Vectors and zinc finger nucleases

Homology-directed repair donor templates were generated from HIV-derived, third-generation self-inactivating transfer constructs. IDLV stocks were prepared as previously described[14] and titered by a Q-PCR designed to discriminate the reverse transcribed vector genome from plasmid carried over from transient transfection[32]. Sequence and maps of *AAVS1-PGK.GFP* were previously reported[22], while *IL2RG-cDNA.PGK.GFP* is described in detail elsewhere (Firrito et al., manuscript in preparation). ZFNs that target intron 1 of *PPP1R12C* or exon 5 of *IL2RG* were previously described[14,16,22,33]. The latter pair was modified to contain high-fidelity obligate heterodimeric FokI variants[34]. Both pairs of ZFNs were transiently expressed as mRNAs. Plasmid templates for ZFNs mRNA production (described in Extended Data Fig. 1b) were linearized and purified by phenol/chloroform extraction followed by ethanol DNA precipitation. 2 μg/reaction of linearized plasmid template was in vitro transcribed at 37 °C for 2 hr using T7 RNA polymerase and 7.5 mM nucleotide triphosphates (MEGAscript Kit; Ambion). Cap0 mRNAs were generated by supplementing the reactions with 6 mM m7(3′-O-methyl)-G(5′)ppp(5′)G, a nonreversible cap analog (ARCA, New England Biolabs) and lowering the concentration of GTP to 1.5 mM. After TURBO DNase treatment (4U/reaction, 1 hr at 37°C), mRNAs were poly(A) tailed with *E. Coli* Poly(A) Polymerase (8U/reaction) for 1 hr at 37°C (PolyA tailing kit; Ambion), yielding ≥ 150 nt polyA. Transcripts were purified by RNeasy Plus Mini Kit (Qiagen). All RNA samples were analyzed by denaturing agarose gel electrophoresis for quality assurance.

In vitro culture and assays on human CB or BM-derived CD34+ cells

CD34+ cells were either freshly purified from human CB after obtaining informed consent and upon approval by the San Raffaele Hospital Bioethical Committee, or purchased frozen from Lonza. 10^6 CD34+ cells/ml were stimulated in serum-free StemSpan medium (StemCell Technologies) supplemented with penicillin, streptomycin and human early-acting cytokines (for CB-derived cells: stem cell factor (SCF) 100 ng/ml, Flt3 ligand (Flt3-L) 100 ng/ml, thrombopoietin (TPO) 20 ng/ml, and interleukin 6 (IL-6) 20 ng/ml; for BM-

Europe PMC Funders Author Manuscripts

derived cells: SCF 300ng/ml, Flt3-L 300 ng/ml, TPO 100 ng/ml, and IL-6 60 ng/ml; all purchased from Peprotech) for 24 or 48 hr and then infected with IDLVs at multiplicity of infection (MOI) 100-500. The following day the cells were electroporated with 175 μg/ml ZFNs encoding mRNAs (P3 Primary Cell 4D-Nucleofector X Kit, program EO-100; Lonza). For some experiments, the following drugs were supplemented to the culture media: 1 μM SR1 (kindly provided by T. Boitano and M. Cooke, GNF) added at every medium change, and 10 μM dmPGE2 (Cayman) added at the beginning of the culture, 1 hour before and just after electroporation. For CFC assays, 800 cells/plate were seeded one day after electroporation in methylcellulose-based medium (MethoCult H4434, StemCell Technologies). Two weeks after plating, colonies were counted and identified according to morphological criteria.

Flow cytometry

For immunophenotypic analysis of CD34+ cells and their progeny (performed on FACSCanto II; BD Pharmingen), we used the antibodies reported in Supplementary Information. Single stained and FMO stained cells were used as controls. For quantitative flow cytometry we used Flow-count Fluorospheres (Beckman Coulter) according to the manufacturers' instructions. Apoptosis analysis was performed on CD34+ cells one day after electroporation using PB-conjugated Annexin V (Biolegend) and Apoptosis Detection Kit with 7-Aminoactinomycin D (7AAD, BD Pharmingen) according to the manufacturers' instructions. Percentages of live (7AAD−, AnnexinV−), early apoptotic (7AAD−, AnnexinV +), late apoptotic (7AAD+, AnnexinV+) and necrotic (7AAD+, AnnexinV−) cells are reported. Cell sorting was performed using MoFlo XDP Cell Sorter (Beckman Coulter).

Molecular analyses

For molecular analyses, genomic DNA was isolated with DNeasy Blood & Tissue Kit or QIAamp DNA Micro Kit (QIAGEN). Extraction of genomic DNA from colonies in CFC assays was performed with Lysis Buffer as previously described[5]. NHEJ in *AAVS1* locus or *IL2RG* gene was detected by the mismatch selective Cel1 assay as previously described[14]. Primers for PCR amplifications to detect targeted integration or for the Cel1 assay are indicated in Supplementary Information. PCR amplicons were resolved on agarose gel and visualized by ethydium bromide staining. For Southern Blot analyses, genomic DNA was extracted with Blood & Cell Culture DNA Midi Kit (QIAGEN) and digested using restriction enzymes (BglI for *AAVS1* locus and BspHI for *IL2RG*) and probes (see Supplementary Information) both located outside of the homology regions included in the vectors. Matched DNA amounts were separated on 1% agarose, transferred to a nylon membrane and probed with ^{32}P-radiolabeled sequences indicated in Supplementary Information. Membranes were exposed in a Storage Phosphor Screen. For Q-PCR analysis, 200 ng of genomic DNA were analyzed using primers and probes complementary to a vector backbone sequence (Primer Binding Site), the GFP sequence and human *TERT*, the latter amplification used as normalizer, as previously described[14]. For gene expression analysis on the SCID-X1 gene corrected colony, mRNA was extracted using RNeasy Micro Kit (QIAGEN) and cDNA was synthetized using SuperScript VILO cDNA Synthesis Kit (Invitrogen). The resulting cDNA was amplified before Q-PCR by Taqman PreAmp Master Mix Kit (Applied Biosystems) according to the manifacturers' instructions. Gene expression

was performed in triplicate with a TaqMan Gene Expression assay specific for the recoded exon 7 of the *IL2RG* gene (Applied Biosystems; see Supplementary Information) in a 7900HT real-time PCR thermal cycler. The relative expression level of the recoded *IL2RG* gene was calculated by the ΔΔCt method and represented as fold change relative to the housekeeping gene control (HPRT), as previously described[22].

Mice transplantation and analysis

For the *in vivo* studies, 8- to 11-week-old NOD-SCID-IL2Rg$^{-/-}$ (NSG) mice were purchased by Jackson laboratory. The experimental protocol was approved by the Institutional Animal Care and Use Committee of the San Raffaele Scientific Institute. At day 4 of culture, 3×10^5 gene targeted CB-derived CD34+ cells (or 7.5×10^5 BM-derived cells) were infused intravenously into the mice after sub-lethal irradiation (200 cGy). Sample size was determined by the total number of available treated cells. Mice were attributed to each experimental group randomly. MDA3 human mammary carcinoma cell line was obtained by stable transduction of MDA-MB 231 cells with lentiviral vectors expressing the human cytokines GM-CSF, IL-7 and IL-15 from the PGK promoter, as previously described[29]. 4×10^6 MDA3 cells were implanted orthotopically in the mammary fat pad of NSG mice 14 weeks after CD34+ cells transplantation or in age-matched untransplanted NSG mice. Human CD45+ engraftment was followed by serial collections of blood from the mouse tail and, at the end of the experiment (12-23 weeks after transplantation), BM and spleen were harvested and analyzed for lineages composition and GFP content (see Supplementary Information for gating strategy).

T lymphocytes analyses

Human T cells were enriched from splenocytes harvested from the transplanted mice using magnetic beads conjugated to anti human CD3 and CD28 antibodies (Dynabeads human T-activator CD3/CD28; Invitrogen), following the manufacturers' instructions, and grown in Iscove's Modified Dulbecco's Media (IMDM) (GIBCO-BRL) supplemented with penicillin, streptomycin, 10% FBS and 5 ng/ml each of IL-7 and IL-15 (PeproTech)[21].

For TCR V-β repertoire analysis, mRNA was extracted from the expanded T cells using RNeasy Mini Kit (QIAGEN) and cDNA was synthetized using SuperScript VILO cDNA Synthesis Kit (Invitrogen). Multiplex PCRs optimized from a previous work [35] were carried out on cDNA using V-β primers specific for 4 or 5 different families and a single FAM-labeled C-β primer. PCR products were fractionated on 6% polyacrylamide gel, visualized on Molecular Dynamics Typhoon 9410 (Amersham Biosciences) and analyzed using ImageQuant TL 7.0 (Amersham Biosciences). V-β complexity was determined by counting the number of distinct peaks and graded on a score of 0–8 [36]. The overall TCR complexity score was determined by summing up all 23 individual TCR V-β family specific scores.

To analyze phosphorylation of downstream effectors of IL2RG pathway, T cells were starved overnight at 37°C in IMDM without cytokines and then stimulated with IL-2 (1000 IU/ml, 100 IU/ml, 10 IU/ml; purchased from Novartis) or IL-15 (10 ng/ml, 5 ng/ml, 1 ng/ml) at 37°C for increasing times. Cells were then fixed in PBS 2% paraformaldehyde (PFA) for 10′ at 37°C, and after washing in PBS 0.1% BSA (3 times), they were

Europe PMC Funders Author Manuscripts

permeabilized with ice-cold absolute methanol for 7′ on ice. After 60′ incubation of each time point of cytokine stimulation with different dilutions of Pacific Blue Succinimidyl Ester (PBSE) (Life Technologies), cells were washed, pooled and stained for flow cytometry.

For proliferation assay, 10^5 T cells were labeled with Cell Proliferation Dye eFluor 670 (eBioscience) according to the manufacturer's instructions. Labeled T cells were co-cultured in IMDM supplemented with penicillin, streptomycin, 10% FBS and 5 ng/ml each of IL-7 and IL-15, with different dilutions of MDA-MB 231 cells previously irradiated at 10000 rad or stimulated for 3 days with PHA (2μg/ml). After 7 days of culture, cells were analyzed by flow cytometry. Division index was calculated according to FlowJo software rules.

For IFN-γ release assay, T cells were stimulated at 37°C for 6 hours with PMA (50ng/ml) and Ionomycin (1μg/ml) in presence of 2μl per ml of culture of BD Golgi Plug (BD Pharmingen). Cells were then fixed and permeabilized using BD Cytofix/Cytoperm Kit (BD Pharmingen) and stained for flow cytometry.

Elispot assay for IFNγ release was performed as previously described[21,29]. When the number of measured spots was above the detection limit of the plate reader (Eli.Expert, A.EL.VIS.), it was arbitrarly set to 500.

Deep sequencing of potential *IL2RG* ZFN off-target loci

Genomic DNA from ZFN-treated CD34+ cells or their progeny harvested from transplanted mice was amplified using REPLI-g Mini Kit (QIAGEN) and the top ranking candidate off-target genomic loci from our previous study[16] amplified by PCR generating amplicons of 389±20 bp surrounding the potential ZFN binding site. PCR products were purified using Agencourt AMPure XP beads (Beckman Coulter) and adaptors were added by TruSeq DNA LT Sample Prep Kit (Illumina). In order to build an equimolar library, PCR products were quantified with KAPA Library Quantification Kit for Illumina sequencing platforms (KAPABIOSYSTEMS) on C1000 Thermal Cycler (BIO-RAD) and sequenced on MiSeq Illumina Platform using MiSeq Reagent v.3 (Illumina). Raw paired-end reads were joined with Fastq-Join program from the EA-Utils NGS suite (http://code.google.com/p/ea-utils/) and aligned to the specific genomic target sequences using Burrows-Wheeler Alignment Tool with maximal exact match version, BWA-MEM [37]. Alignments were evaluated and filtered using SAMtools [38], Picard (http://picard.sourceforge.net) and BAMtools[39]. Sequences with only primary alignments with quality > 15 were kept for further analysis. Deletions and insertions (indels) were quantified by a custom pipeline based on Python (http://www.python.org, version 2.7.6) and the PySAM library (https://code.google.com/p/pysam, version 0.7.5). Sequences with indels of ≥1 bp located within a region encompassing the spacer + 5 bp on each side were considered as ZFN-induced genome modifications. Coverage statistics were computed by the binomial distribution online calculator (http://www.vassarstats.net/binomialX.html). Fisher exact test were computed with the SciPy Python package (http://www.scipy.org, version 0.9.0) within the "stats" library. Multiple sequence alignment for indels visualization and plot was performed with ClustalW2[40] and MView (http://bio-mview.sourceforge.net/).

Europe PMC Funders Author Manuscripts

SCID-X1 cells

Peripheral blood and bone marrow samples from a subject with SCID-X1 were obtained according to the guidelines of the Medical Ethics Committee of the Erasmus MC, University Medical Center Rotterdam, the Netherlands.

Statistical analyses

Statistical analyses were performed by unpaired Student's t test for pairwise comparison or one-way or two-way analysis of variance (ANOVA) with Bonferroni's multiple comparison post-test for three or more groups, as indicated. Values are expressed as Mean ± standard error of the mean (SEM). Percent values were transformed into a log-odds scale (log (%x/(100-%x)) to perform statistical analyses.

Supplementary Material

Refer to Web version on PubMed Central for supplementary material.

Acknowledgments

We thank D. Weissman (University of Pennsylvania) for advices on mRNA production and the whole Naldini laboratory for fruitful discussion, F. Benedicenti for help with MiSeq sequencing, L. Sergi Sergi, T. Plati, V. Valtolina, B. Camisa and A. Ranghetti for technical help. SR1 was kindly provided by T. Boitano and M. Cooke under an MTA with the Genomics Institute of the Novartis Research Foundation. This work was supported by grants to L.N. from Telethon (TIGET grant D2) EU (FP7 222878 PERSIST, FP7 601958 SUPERSIST, ERC Advanced Grant 249845 TARGETINGGENETHERAPY) and the Italian Ministry of Health.

References of the main text

1. Mukherjee S, Thrasher AJ. Gene therapy for PIDs: progress, pitfalls and prospects. Gene. 2013; 525:174–181. doi:10.1016/j.gene.2013.03.098. [PubMed: 23566838]
2. Aiuti A, et al. Lentiviral Hematopoietic Stem Cell Gene Therapy in Patients with Wiskott-Aldrich Syndrome. Science. 2013; 341:1233151. doi:10.1126/science.1233151. [PubMed: 23845947]
3. Cavazzana-Calvo M, et al. Transfusion independence and HMGA2 activation after gene therapy of human beta-thalassaemia. Nature. 2010; 467:318–322. doi:10.1038/nature09328. [PubMed: 20844535]
4. Cartier N, et al. Hematopoietic stem cell gene therapy with a lentiviral vector in X-linked adrenoleukodystrophy. Science. 2009; 326:818–823. [PubMed: 19892975]
5. Biffi A, et al. Lentiviral Hematopoietic Stem Cell Gene Therapy Benefits Metachromatic Leukodystrophy. Science. 2013; 341:1233158. doi:10.1126/science.1233158. [PubMed: 23845948]
6. Naldini L. Ex vivo gene transfer and correction for cell-based therapies. Nature reviews. Genetics. 2011; 12:301–315. doi:10.1038/nrg2985.
7. Braun CJ, et al. Gene therapy for wiskott-Aldrich syndrome--long-term efficacy and genotoxicity. Science translational medicine. 2014; 6:227ra233. doi:10.1126/scitranslmed.3007280.
8. Cavazza A, Moiani A, Mavilio F. Mechanisms of retroviral integration and mutagenesis. Human gene therapy. 2013; 24:119–131. doi:10.1089/hum.2012.203. [PubMed: 23330935]
9. Woods NB, Bottero V, Schmidt M, von Kalle C, Verma IM. Gene therapy: therapeutic gene causing lymphoma. Nature. 2006; 440:1123. [PubMed: 16641981]
10. Gentner B, et al. Identification of hematopoietic stem cell-specific miRNAs enables gene therapy of globoid cell leukodystrophy. Science translational medicine. 2010; 2:58ra84. doi:10.1126/scitranslmed.3001522.
11. Urnov FD, Rebar EJ, Holmes MC, Zhang HS, Gregory PD. Genome editing with engineered zinc finger nucleases. Nature reviews. 2010; 11:636–646. doi:10.1038/nrg2842.

12. Joung JK, Sander JD. TALENs: a widely applicable technology for targeted genome editing. Nature reviews. Molecular cell biology. 2013; 14:49–55. doi:10.1038/nrm3486. [PubMed: 23169466]
13. Sander JD, Joung JK. CRISPR-Cas systems for editing, regulating and targeting genomes. Nature biotechnology. 2014; 32:347–355. doi:10.1038/nbt.2842.
14. Lombardo A, et al. Gene editing in human stem cells using zinc finger nucleases and integrase-defective lentiviral vector delivery. Nat Biotechnol. 2007; 25:1298–1306. doi:10.1038/nbt1353. [PubMed: 17965707]
15. Urnov FD, et al. Highly efficient endogenous human gene correction using designed zinc-finger nucleases. Nature. 2005; 435:646–651. doi:10.1038/nature03556. [PubMed: 15806097]
16. Gabriel R, et al. An unbiased genome-wide analysis of zinc-finger nuclease specificity. Nat Biotechnol. 2011; 29:816–823. doi:10.1038/nbt.1948. [PubMed: 21822255]
17. Mussolino C, et al. A novel TALE nuclease scaffold enables high genome editing activity in combination with low toxicity. Nucleic acids research. 2011; 39:9283–9293. doi:10.1093/nar/gkr597. [PubMed: 21813459]
18. Ciccia A, Elledge SJ. The DNA damage response: making it safe to play with knives. Molecular cell. 2010; 40:179–204. doi:10.1016/j.molcel.2010.09.019. [PubMed: 20965415]
19. Tebas P, et al. Gene editing of CCR5 in autologous CD4 T cells of persons infected with HIV. N Engl J Med. 2014; 370:901–910. doi:10.1056/NEJMoa1300662. [PubMed: 24597865]
20. Holt N, et al. Human hematopoietic stem/progenitor cells modified by zinc-finger nucleases targeted to CCR5 control HIV-1 in vivo. Nat Biotechnol. 2010; 28:839–847. doi:10.1038/nbt.1663. [PubMed: 20601939]
21. Provasi E, et al. Editing T cell specificity towards leukemia by zinc finger nucleases and lentiviral gene transfer. Nat Med. 2012; 18:807–815. doi:10.1038/nm.2700. [PubMed: 22466705]
22. Lombardo A, et al. Site-specific integration and tailoring of cassette design for sustainable gene transfer. Nature methods. 2011; 8:861–869. doi:10.1038/nmeth.1674. [PubMed: 21857672]
23. Zou J, et al. Oxidase-deficient neutrophils from X-linked chronic granulomatous disease iPS cells: functional correction by zinc finger nuclease-mediated safe harbor targeting. Blood. 2011; 117:5561–5572. doi:10.1182/blood-2010-12-328161. [PubMed: 21411759]
24. Li H, et al. In vivo genome editing restores haemostasis in a mouse model of haemophilia. Nature. 2011; 475:217–221. doi:10.1038/nature10177. [PubMed: 21706032]
25. Doulatov S, Notta F, Laurenti E, Dick JE. Hematopoiesis: a human perspective. Cell stem cell. 2012; 10:120–136. doi:10.1016/j.stem.2012.01.006. [PubMed: 22305562]
26. Boitano AE, et al. Aryl hydrocarbon receptor antagonists promote the expansion of human hematopoietic stem cells. Science. 2010; 329:1345–1348. doi:10.1126/science.1191536. [PubMed: 20688981]
27. North TE, et al. Prostaglandin E2 regulates vertebrate haematopoietic stem cell homeostasis. Nature. 2007; 447:1007–1011. doi:10.1038/nature05883. [PubMed: 17581586]
28. Goessling W, et al. Prostaglandin E2 enhances human cord blood stem cell xenotransplants and shows long-term safety in preclinical nonhuman primate transplant models. Cell stem cell. 2011; 8:445–458. doi:10.1016/j.stem.2011.02.003. [PubMed: 21474107]
29. Escobar G, et al. Genetic engineering of hematopoiesis for targeted IFN-alpha delivery inhibits breast cancer progression. Science translational medicine. 2014; 6:217ra213. doi:10.1126/scitranslmed.3006353.
30. Milyavsky M, et al. A distinctive DNA damage response in human hematopoietic stem cells reveals an apoptosis-independent role for p53 in self-renewal. Cell stem cell. 2010; 7:186–197. doi:10.1016/j.stem.2010.05.016. [PubMed: 20619763]
31. Mohrin M, et al. Hematopoietic stem cell quiescence promotes error-prone DNA repair and mutagenesis. Cell stem cell. 2010; 7:174–185. doi:10.1016/j.stem.2010.06.014. [PubMed: 20619762]

Europe PMC Funders Author Manuscripts

Additional References

32. Matrai J, et al. Hepatocyte-targeted expression by integrase-defective lentiviral vectors induces antigen-specific tolerance in mice with low genotoxic risk. Hepatology. 2011; 53:1696–1707. doi: 10.1002/hep.24230. [PubMed: 21520180]
33. Hockemeyer D, et al. Efficient targeting of expressed and silent genes in human ESCs and iPSCs using zinc-finger nucleases. Nat Biotechnol. 2009; 27:851–857. doi:10.1038/nbt.1562. [PubMed: 19680244]
34. Miller JC, et al. An improved zinc-finger nuclease architecture for highly specific genome editing. Nat Biotechnol. 2007; 25:778–785. [PubMed: 17603475]
35. Akatsuka Y, Martin EG, Madonik A, Barsoukov AA, Hansen JA. Rapid screening of T-cell receptor (TCR) variable gene usage by multiplex PCR: application for assessment of clonal composition. Tissue Antigens. 1999; 53:122–134. [PubMed: 10090612]
36. Wu CJ, et al. Reconstitution of T-cell receptor repertoire diversity following T-cell depleted allogeneic bone marrow transplantation is related to hematopoietic chimerism. Blood. 2000; 95:352–359. [PubMed: 10607724]
37. Li H, Durbin R. Fast and accurate short read alignment with Burrows-Wheeler transform. Bioinformatics. 2009; 25:1754–1760. doi:10.1093/bioinformatics/btp324. [PubMed: 19451168]
38. Li H, et al. The Sequence Alignment/Map format and SAMtools. Bioinformatics. 2009; 25:2078–2079. doi:10.1093/bioinformatics/btp352. [PubMed: 19505943]
39. Barnett DW, Garrison EK, Quinlan AR, Stromberg MP, Marth GT. BamTools: a C++ API and toolkit for analyzing and managing BAM files. Bioinformatics. 2011; 27:1691–1692. doi:10.1093/bioinformatics/btr174. [PubMed: 21493652]
40. Larkin MA, et al. Clustal W and Clustal X version 2. Bioinformatics. 2007; 23:2947–2948. doi: 10.1093/bioinformatics/btm404. [PubMed: 17846036]
41. Harris DT, Badowski M, Balamurugan A, Yang OO. Long-term human immune system reconstitution in non-obese diabetic (NOD)-Rag (-)-gamma chain (-) (NRG) mice is similar but not identical to the original stem cell donor. Clin Exp Immunol. 2013; 174:402–413. doi:10.1111/cei.12192. [PubMed: 24032450]
42. Gattinoni L, et al. A human memory T cell subset with stem cell-like properties. Nature Medicine. 2011; 17:1290–1297. doi:10.1038/nm.2446.
43. Cieri N, et al. IL-7 and IL-15 instruct the generation of human memory stem T cells from naive precursors. Blood. 2013; 121:573–584. doi:10.1182/blood-2012-05-431718. [PubMed: 23160470]

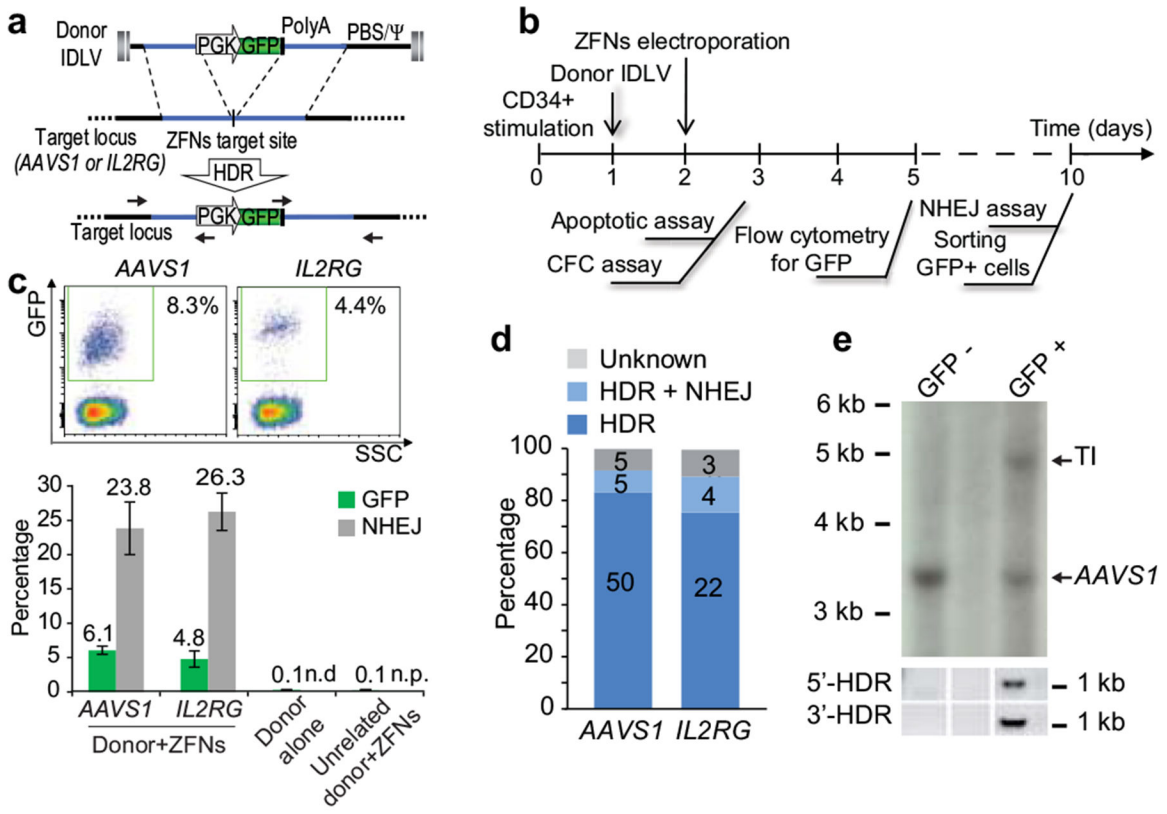

Figure 1. Targeted integration into *AAVS1* or *IL2RG* in CB CD34+ cells

a, Schematic of the donor IDLV template containing a GFP cassette driven by the phosphoglycerate kinase promoter (PGK) flanked by sequences homologous to the genomic target locus, the target locus with the ZFNs cleavage site and the locus after HDR showing the PCR primers used to assess 5′ or 3′ HDR-mediated integration junctions (black arrows). **b**, Flow chart for targeted integration (TI) and cell analyses. **c**, Representative flow cytometry dot plots (Top) and percentages of GFP+ cells and NHEJ-induced indels at the target locus (Bottom) of CB CD34+ cells treated for TI into *AAVS1* or *IL2RG*. Means ± SEM (*AAVS1*, n=39 on 19 CB donors; *IL2RG*, n=10 on 9 CB donors). Unrelated donor: cells treated with IDLV lacking homology to the target site. nd: not detectable, np: not performed. **d**, Targeting specificity in CFC. Percentage of colonies positive for both (HDR), either (HDR+NHEJ) or none (Unknown) 5′ and 3′ HDR junctions by PCR. Numbers of colonies screened indicated inside the bars. **e**, Southern blot (top) and PCR (bottom) analyses of iPSC obtained by reprogramming GFP+ or GFP− cells from (**c**).

Europe PMC Funders Author Manuscripts

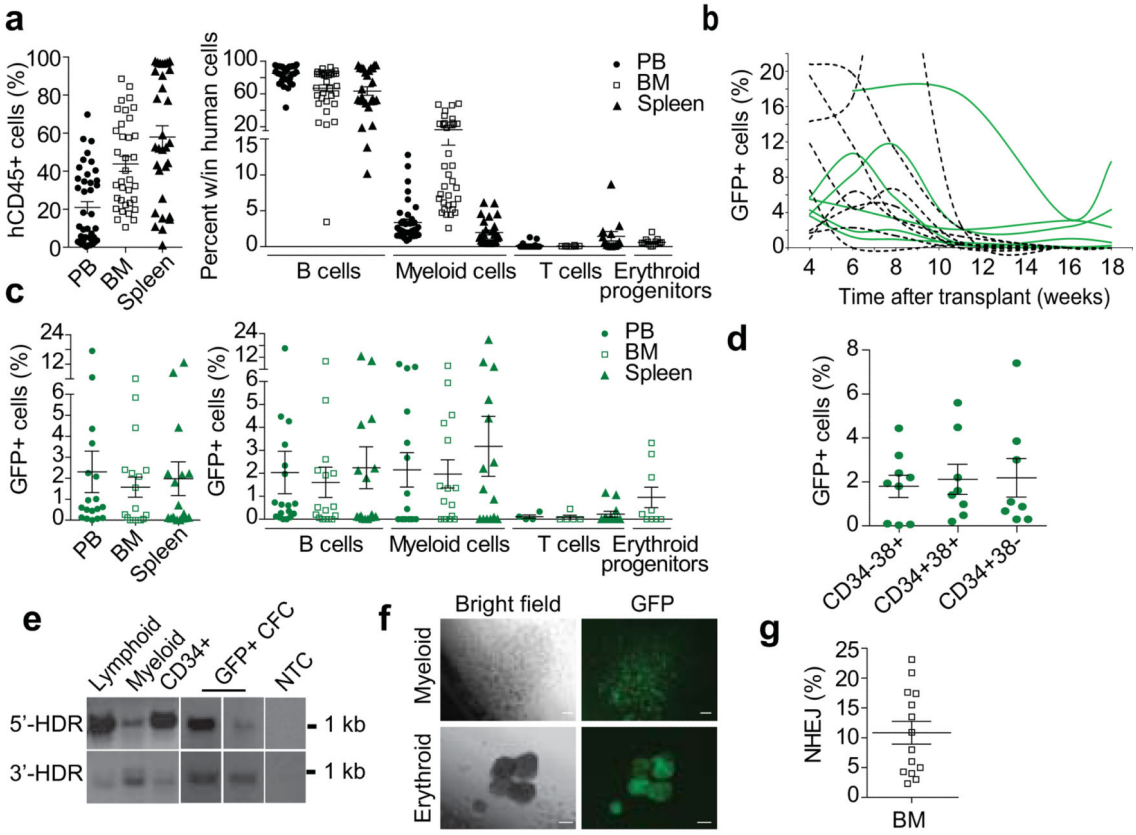

Figure 2. Transplantation of gene targeted CD34+ cells in NSG mice

CD34+ cells treated as in Fig.1b were transplanted into NSG mice. **a**, (Left) Human cell engraftment (CD45+) 12-23 weeks post-transplant in the indicated organs. (Right) Percentages of the indicated lineages within the human graft. Data from individual mice and mean ± SEM (n=42 mice; 6 independent experiments on 13 CB donors). **b**, Time course of human GFP+ cells in PB of mice. Dashed lines: mice in which GFP+ cells were no longer detectable (<0.1%) 12 weeks post-transplant. **c**, GFP+ cells within the human graft in the indicated organs (Left) and lineages (Right). (n=18). **d**, GFP+ cells within human primitive (CD34+CD38−) or committed (CD34+CD38+) progenitors or differentiated cells (CD34-CD38+) in mouse BM. **e**, PCR analysis for TI into *AAVS1* on human lymphoid (CD19+) and myeloid (CD33+ and CD13+) cells sorted from the mice and on GFP+ CFC from mouse BM. **f**, Representative images of GFP+ colonies. Scale bars, 0.5 mm. **g**, NHEJ at *AAVS1* or *IL2RG* ZFNs target sites on total BM cells from (**a**). n= 25, 3 independent experiments.

Europe PMC Funders Author Manuscripts

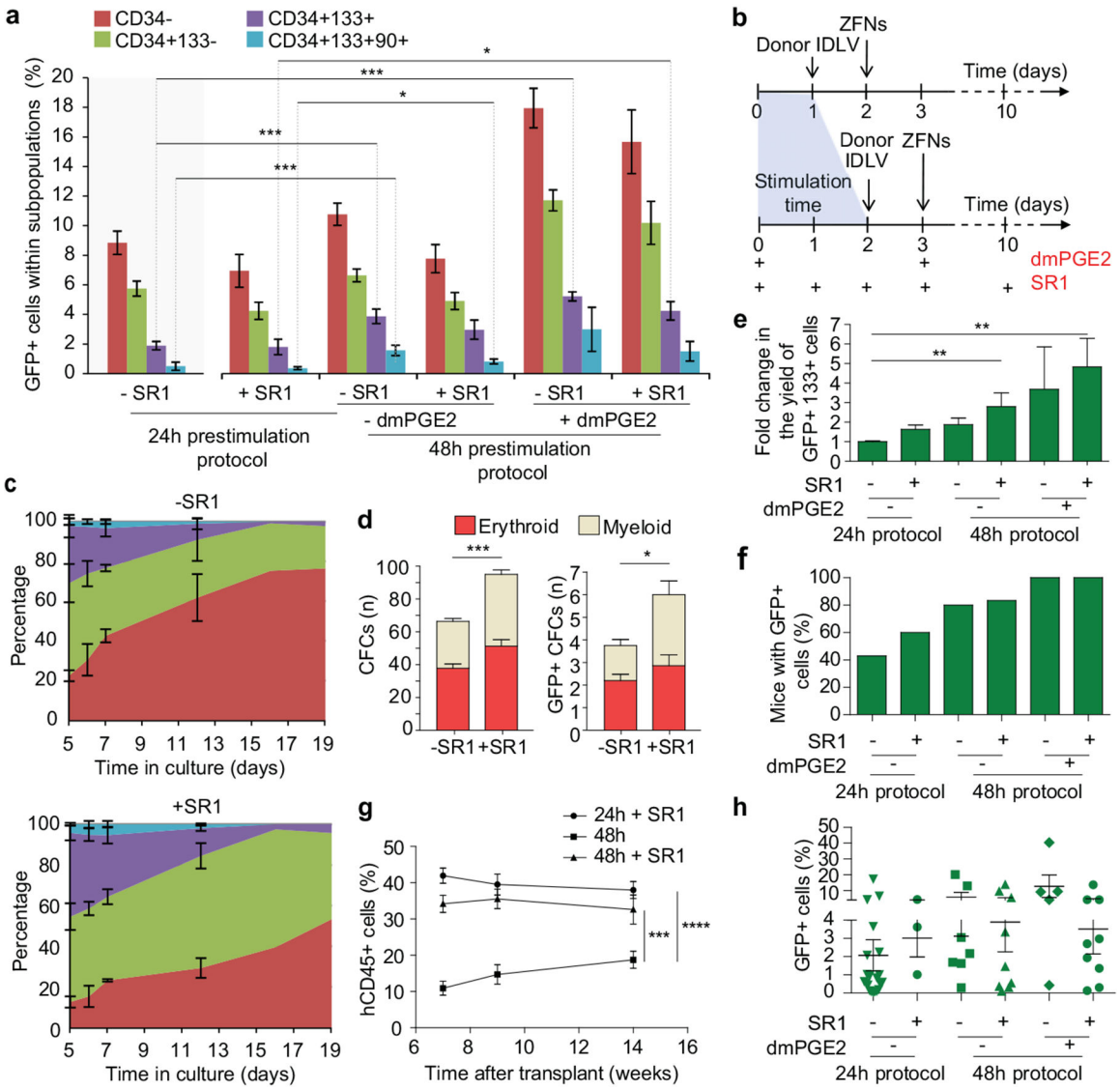

Figure 3. Gene targeting in primitive *versus* committed progenitors

a, GFP+ cells within the indicated subpopulations 3 days after treatment for TI. The left most panel shows results using the protocol described in Fig.1b. The other panels show the effect of longer prestimulation and/or addition of the indicated drugs, as shown in the schematic in (**b**). Means ± SEM (n=31,15,14,15,7,5 respectively on 37 total CB donors). *p< 0.05; ***p< 0.001 (one-way Anova). **c**, Composition of CD34+ cells cultured with or without SR1; subpopulations as in (**a**) . Means ± SEM (n=4). **d**, Total (left) and GFP+ (right) colonies from CD34+ cells treated for TI with or without SR1. Means ± SEM (n=20, 14). **e**, Yield of GFP+ early progenitors relative to that obtained using the original protocol of Fig.1b. Means ± SEM (n=8,7,11,10,3,5) **p<0.01 (one-way Anova). **f**, Percentage of NSG mice harboring GFP+ cells 14 weeks after transplant of CD34+ cells treated with the indicated TI protocols. **g**, Time course of human engraftment in PB. Means ± SEM (24h SR1, n=5; 48h SR1, n=6; 48h, n=5) ****p<0.0001, ***p<0.001 (two-way Anova). **h**, GFP+

Europe PMC Funders Author Manuscripts

cells within CD45+ cells in PB 14 weeks post-transplant. Means ± SEM (n=4). Mice for the 24h SR1- condition are shown for comparison from Fig.2c.

Europe PMC Funders Author Manuscripts

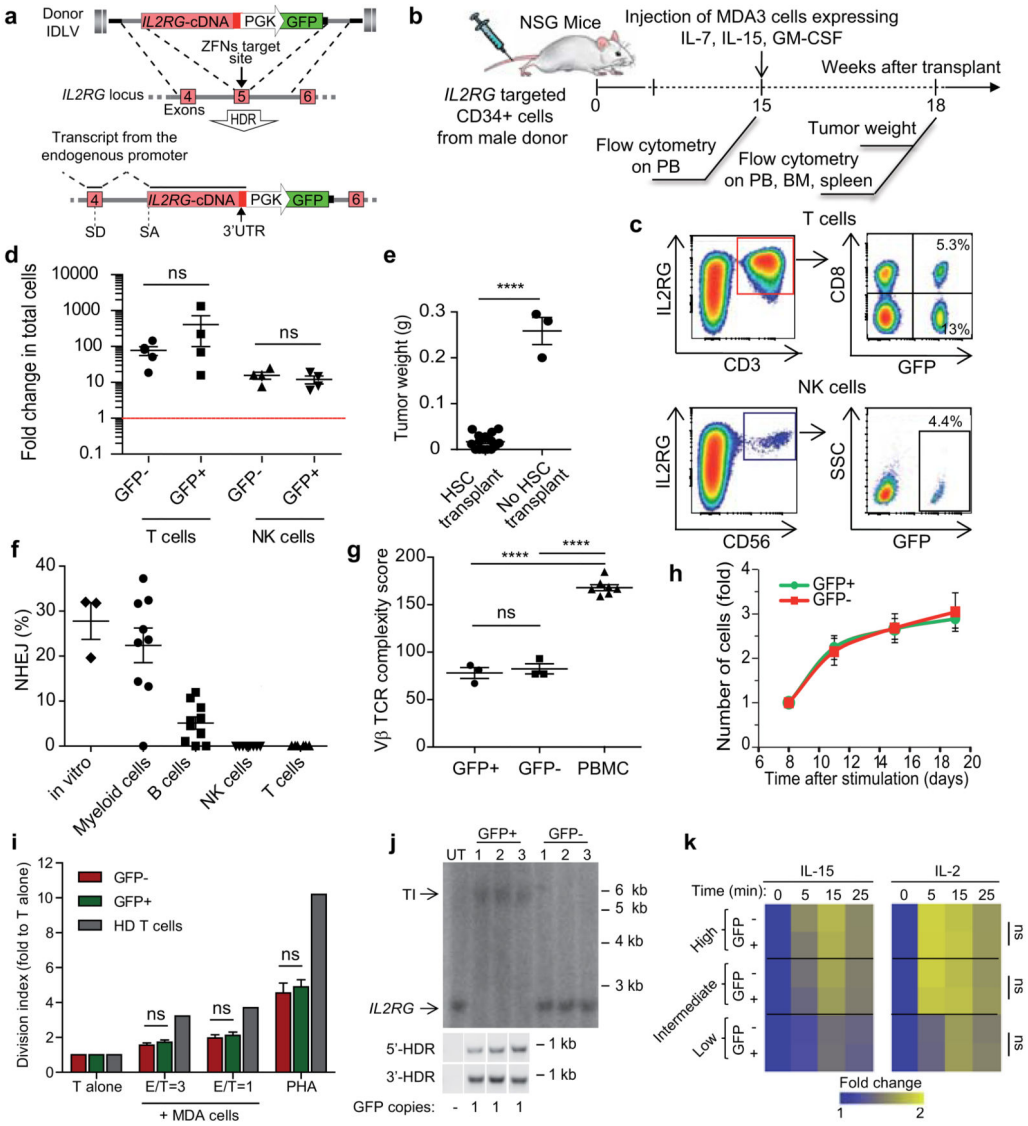

Figure 4. Functional reconstitution of *IL2RG* in the lymphoid progeny of HSC

a, Schematic of the *IL2RG* donor: a promoter-less *IL2RG* cDNA, comprising exons 5-8 plus 3′ untranslated region (UTR), and a PGK-GFP cassette are flanked by homologous sequences to those surrounding the *IL2RG* ZFNs target site. **b**, Flow chart of cell transplantation, tumor challenge and analyses. **c**, Density plots of γ-chain expressing T (Top) and NK (Bottom) cells showing GFP marking. (n=7,11). **d**, Expansion of GFP− and GFP+ T and NK cells after tumor challeng. **e**, Tumor weight 3 weeks after challenge, in mice transplanted (n=16) or not (n=3). ****p<0.0001 (unpaired t test). **f**, NHEJ in the *IL2RG* gene on CD34+ cells cultured *in vitro* and on their progeny sorted from the transplanted mice. **g**, TCR complexity score calculated on GFP+ or GFP− T cells from transplanted mice. Human PB mononuclear cells (PBMCs) were used as positive control. ****p<0.0001 (one-way Anova). **h**, *Ex vivo* growth of GFP+ and GFP− T cells from the spleen of transplanted mice upon stimulation (n= 4). **i**, Division index of GFP+ or GFP− T cells 7 days after PHA

stimulation or co-culture with tumor cells at the indicated effector-to-target (E/T) ratios. p=ns (unpaired t test). T cells from healthy donor (HD) were used as controls. **j**, Southern blot (top), PCR (middle) and GFP q-PCR (bottom) analyses showing TI of the corrective *IL2RG* cDNA in sorted GFP+ T cells from (**h**). UT: untreated cells. **k**, Heatmap showing changes in phosphorylation levels of STAT5 after the indicated time of exposure to decreasing amounts of IL-2 or IL-15, on T cells from (**h**). p=ns (two-way Anova).

Europe PMC Funders Author Manuscripts

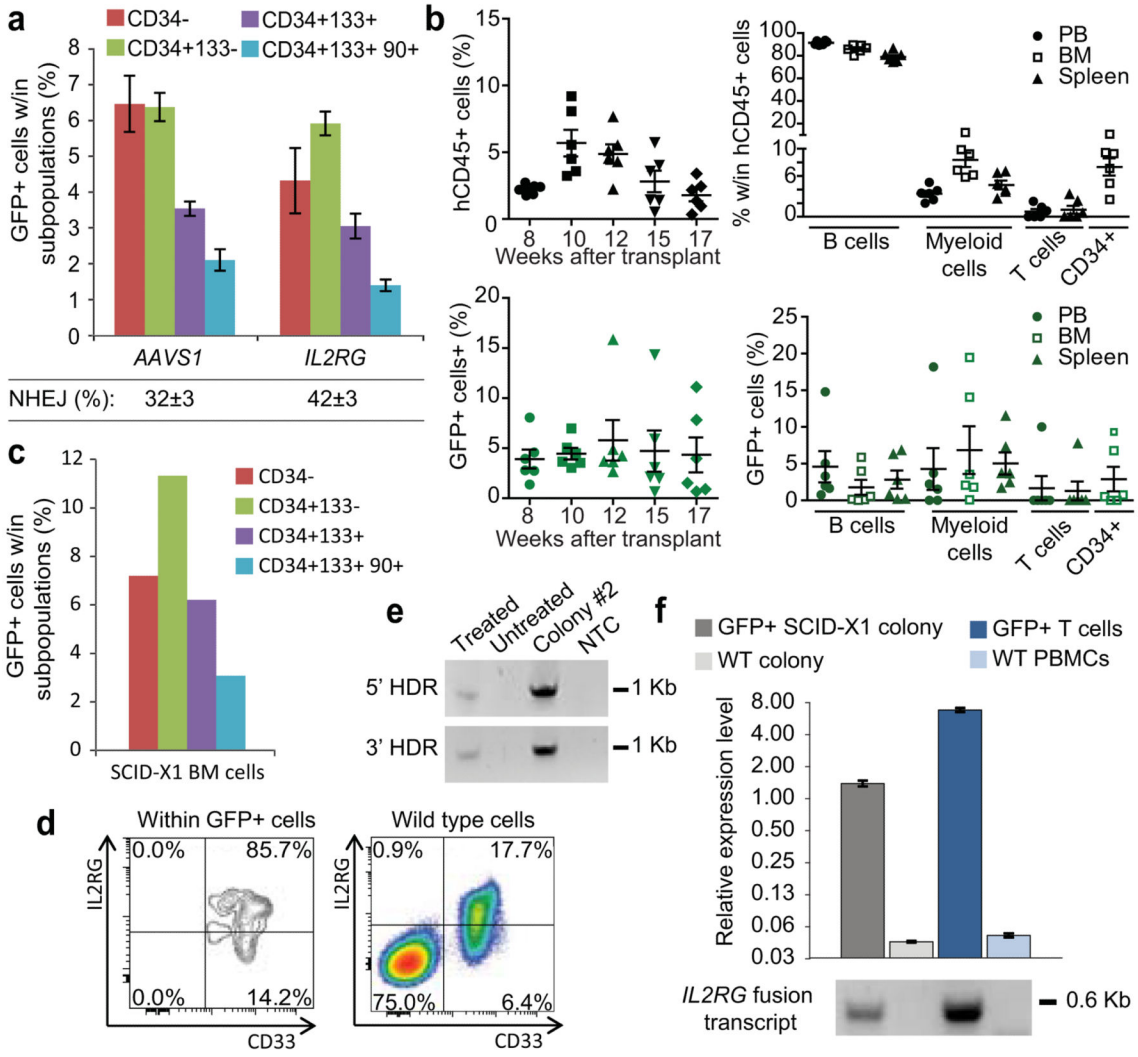

Figure 5. Targeted integration and *IL2RG* gene correction in BM-derived CD34+ cells from healthy donors and a subject with SCID-X1

a, (Top) GFP+ cells within the indicated subpopulations derived from BM CD34+ cells of adult healthy donors, treated for TI according to the best performing protocol from Fig. 3. (Bottom) NHEJ at the ZFN target site on total cells. Means ± SEM, (n=10,3 from 4,3 donors for *AAVS1* or *IL2RG*, respectively) **b**, (Top left) Human cells in PB of NSG mice transplanted with cells from (**a**). (Top right) Percentages of the indicated lineages within human cells 15 weeks post-transplant. (Bottom) GFP+ cells within the indicated populations. **c**, GFP+ cells measured as in (**a**) in BM CD34+ cells from a subject with SCID-X1 treated for *IL2RG* gene correction. **d**, IL2RG expression on myeloid (CD33+) cells from a GFP+ colony from the cells treated in (**c**) or from pooled wild type colonies. **e**, PCR analysis for TI into *IL2RG* of the corrective cDNA on cells from (**c**) and (**d**). **f**, Expression of the fusion transcript bearing the corrective *IL2RG* cDNA measured by Q-PCR (top) or RT-PCR (bottom) on cDNA from a GFP+ SCID-X1 myeloid colony. *IL2RG* targeted T cells

Europe PMC Funders Author Manuscripts

from engrafted mice analyzed in Fig. 4j were used as positive control, while a myeloid colony from wild-type BM cells (WT) and PBMCs were used as negative controls.

Europe PMC Funders Author Manuscripts

Table 1

Indels quantification on the target and candidate off target sites of *IL2RG* ZFNs in the progeny of treated CD34+ cells

In/Ex indicates whether the ZFN target site is within an exon (Ex), intron (In) or intergenic (Outside) near to the RefSeg gene indicated in the first column.Homology: percent of sequence identity to the *IL2RG*-ZFNs binding sites. ZFN-Dimer: the site can be bound by a homodimeric (LL/RR) or heterodimeric (LR/RL) ZFN pair. Number indicates the spacer length in bpbetween the ZFN binding sites. NHEJ (%): percent of indels on treated CD34+ cells cultured *in vitro* (sample A, B and G) and on human cells harvested from the BM of long-term engrafted NSG mice from Fig. 3 (mouse B2, C0 and E2). For quantification see Supplementary Information and Extended Data Fig. 9. Ns: not significant (Fisher exact test for contingency data).

Nearest RefSeq gene	In/Ex	Homology (%)	ZFN-Dimer	NHEJ (%)					
				In vitro			Engrafted in Mouse		
				A	B	G	B2	C0	E2
IL2RG	Ex	100	L_5_R	54.60	61.18	45.60	26.08	43.51	20.07
SCARB1	Outside	70.8	L_5_R	0.17	0.70	ns	ns	ns	ns
SLC31A1	In	75	R_5_L	0.61	ns	ns	ns	0.02	ns
FAM133B	In	66.7	R_6_R	ns	ns	ns	ns	ns	ns
KIAA0528	In	87.5	L_5_L	ns	ns	ns	ns	ns	ns
SF3B1	Outside	66.7	L_5_L	ns	ns	ns	ns	ns	ns
A2BP1	Outside	75	L_5_R	ns	ns	ns	ns	ns	ns
ANKFY1	Ex	87.5	L_3_R	ns	ns	ns	ns	ns	ns
TRIM43	Outside	91.7	L_4_L	ns	ns	ns	ns	ns	ns
SEC16A	Ex	70.8	R_6_L	ns	ns	ns	ns	ns	ns